

Optimizing Vibrational Population Transfer at Surfaces through Infrared Excitation

Mischa Bonn* **and Martin Wolf**†,#

Leiden Institute of Chemistry, P.O. Box 9502, 2300 RA Leiden, The Netherlands

†Freie Universität Berlin, Institut für Experimentalphysik, Arnimalle 14, 14195 Berlin, Germany

(Received September 17, 2001)

We present an experimental and theoretical study of vibrational excitation of the C–O stretch vibration of carbon monoxide adsorbed on a ruthenium Ru(001) surface with ultrashort femtosecond infrared (IR) laser pulses. Broadband IR excitation leads to the transfer of a significant fraction of the CO molecules to their first (∼15%) and second (∼5%) vibrationally excited states. We reproduce the observed excited state spectra by solving the three-level Bloch equations and discuss possibilities to optimize the degree of localized vibrational excitation of a specific bond of surface molecules through IR excitation by tuning the pulse duration and central frequency.

Mode selective chemistry has been one of the long-time goals in physical chemistry. It has long been recognized that in achieving control over chemical reactions on a molecular level, the vibrational state of a molecule plays a key role: excitation of a specific vibrational mode is an important aspect of state-selective chemistry. Indeed, control over the outcome of a chemical reaction by mode-specific vibrational excitation has been demonstrated in detail in the gas phase. For instance, the outcome of the reaction between a hydrogen atom and (deuterated) water to give H_2 (HD) and OH (OD), can be controlled to a large extent by bond-specifically vibrationally exciting either the O–H or the O–D stretch vibration of the reactant water[1–3]; the bond that is vibrationally excited preferentially reacts. Moreover, a high degree of excitation (to high-lying levels of specific vibrational states) will increase the selectivity. Due to the anharmonicity of the vibrational ladder, broad-band infrared laser sources are ideally suited for the "vibrational ladder-climbing" process.[4,5] In addition, these short laser pulses have the advantage that the energy is inserted into the system faster than vibrational relaxation (IVR) and energy redistribution can occur, so that the energy remains localized in the relevant coordinate long enough for the subsequent chemical reaction to occur. This is particularly important for larger molecules and, as will be demonstrated below, for molecules on surfaces. Indeed, it has been demonstrated for gas-phase NO (N–O stretch)[6] and $W(CO)_6$ (C–O stretch) in solution[7] that ultrashort infrared pulses can be used to transfer population up to the highest level of the N–O stretch vibration within reach of the IR bandwidth, i.e. up to $v = 5$.

For molecules on metal surfaces, reaching high levels of vibrational excitation is complicated by the efficient vibrational energy relaxation which occurs by electron-hole pair excitation in the metal, typically on a picosecond time scale.[8,9] This means that there will be competition between excitation and de-excitation, especially relevant for picosecond pulses. This would indicate that shorter pulses would be better for vibrational ladder climbing, also considering that the anharmonicity of the potential requires sufficient spectral bandwidth for efficient vibrational ladder-climbing. However, on the other hand, decreasing the duration of the excitation pulse leads to more spectral bandwidth, and therefore a reduced spectral brightness at the transition that must be excited; the reduced spectral brightness of these short pulses will reduce the transition probability. In this paper, we address these competing effects.

We investigate the dynamics of the C–O stretch vibration of carbon monoxide absorbed on a Ru(001) surface by IR–Vis–Sum Frequency Generation (SFG).[10] We demonstrate that, after vibrational excitation with ultrashort infrared pulses, a considerable amount of CO molecules can be excited to their second vibrationally excited state. The resulting excited states spectra can be reproduced very well using the three-level optical Bloch equations that describe the time evolution of the vibrational polarization and population. Subsequently, we theoretically investigate the effect of variation of the IR pulse duration and central frequency on the excited state population and excited state spectra. We observe a competition between the high intensities of very short pulses, and the high spectral brightness of long pulses, resulting in an optimal pulse duration of a few hundred femtoseconds for population in the second excited state. The effects of chirped pulse excitation[11,12] and energy delocalization as a consequence of dipole–dipole coupling[13,14] have been described in a previous manuscript.[15]

Experimental

The experiments were performed with a femtosecond laser system combined with an ultra-high vacuum (UHV) chamber. An optical parametric amplifier (TOPAS, Light Conversion) pumped by 4 mJ of an amplified Ti:Sapphire laser system is used to generate tunable mid-IR pulses (2–10 μm, at 5 μm wavelength ∼ 130 fs pulses with energies up to 25 μJ and a bandwidth of typically 100–120 cm^{-1} (FWHM) are obtained). In addition a narrow-band-

Fritz-Haber-Institut der Max-Planck-Gesellschaft, Faradayweg 4–6, 14195 Berlin, Germany

width (5–8 cm^{-1}) vis-pulse at 800 nm is generated. For the SFG experiments the IR and vis pulses are spatially and temporally overlapped and focussed into the UHV chamber under 70° with respect to the surface normal. Typical pulse energies are 4 μJ for the VIS and up to 11 μJ for the IR pulses at the sample (beam waist at focus: 0.3 mm FWHM). The center frequency of the IR is resonant with the C–O strech vibration.

SFG is a second-order non-linear optical process in which two incident waves at ω_{vis} and ω_{IR} generate an output at $\omega_{SFG} = \omega_{vis} + \omega_{IR}$ where energy and momentum must be conserved.[10] When using broadband-IR pulses, resonant enhancement will only occur for frequencies ω_{IR} within the bandwidth which are resonant with the vibrational transition. Thus, vibrational spectra can be obtained without scanning the IR frequency.[16–18] The SFG beam is focussed into a spectrograph and dispersed across an intensified CCD detector.

The Ru(001) sample is mounted in a UHV chamber (base pressure 1×10^{-8} Pa) and can be cooled to 95 K. An extensive description of the complete experimental setup and surface cleaning procedures can be found in Ref. 19. CO exposure was performed via a pinhole doser or a variable leak valve. The CO coverage is determined by comparing the integrated desorption yield with thermal desorption spectra obtained after saturating the Ru surface with CO (0.68 ML[20]).

Results

The upper panel of Fig. 1 depicts SFG spectra as a function of infrared intensity at a surface coverage of approximately 0.01 monolayers and a temperature of 95 K. The coverage was kept sufficiently low to avoid effects of intermolecular coupling on the SFG spectra.[14] At low IR energies, a Lorentzian resonance is observed associated with the transition from the ground ($v = 0$) to the first excited ($v = 1$) state. With increasing energy the fundamental transition ($v = 0 \rightarrow 1$) is saturated, and significant population is transferred to the ($v = 1$) state. An additional interaction with the broad-band infrared field gives rise to a polarization at the ($v = 1 \rightarrow 2$) transition, from which SFG is generated at a slightly lower frequency due to the anharmonicity (~30 cm^{-1}) of the vibrational potential. This effect exhibits a strong non-linear dependence on the infrared pulse energy (as it is a fourth-order ($\chi^{(4)}$) non-linear optical process, see below), which is obvious from Fig. 1: With increasing IR power the $v = 1 \rightarrow 2$ hot band of the CO-stretch vibration becomes clearly visible at 1961.4 ± 0.3 cm^{-1}, in addition to the fundamental transition at 1990.4 ± 0.1 cm^{-1} which is also observed at lower IR energies. The third resonance around 1938 cm^{-1} arises from two contributions: The $v = 2 \rightarrow 3$ hot-band and the fundamental transition of the naturally abundant $^{13}C^{16}O$ in $^{12}C^{16}$ gas. The SFG spectra $I_{SFG}(\omega)$ can be reproduced very well by an expression for the second-order non-linear susceptibility consisting of a nonresonant term $\chi^{(2)}_{NR}$ arising from the surface region of the metal and a resonant term $\chi^{(2)}_{R}$ associated with the vibrational transition:[21,22]

$$I_{SFG}(\omega) \propto \left|\chi^{(2)}\right|^2;\ \chi^{(2)} = \chi^{(2)}_{NR} + \chi^{(2)}_{R};$$
$$\chi^{(2)}_{NR} = A_0 e^{i\phi};\ \chi^{(2)}_{R} = \sum_n \frac{A_n}{\omega_{IR} - \omega_n + i\Gamma_n} \quad (1)$$

where the vibrational resonances are described by their resonance frequencies ω_n, linewidths $2\Gamma_n$ and amplitudes A_n, so that the $\chi^{(4)}$ contribution is incorporated in $\chi^{(2)}$. A_0 is the amplitude of the nonresonant susceptibility and ϕ its phase relative to the vibrational resonance. The dotted lines in the upper panel of Fig. 1 depict the fit to the experimental data using this procedure. The dotted lines in the lower panel show the resonant contribution to the non-linear susceptibility as obtained from the fit.

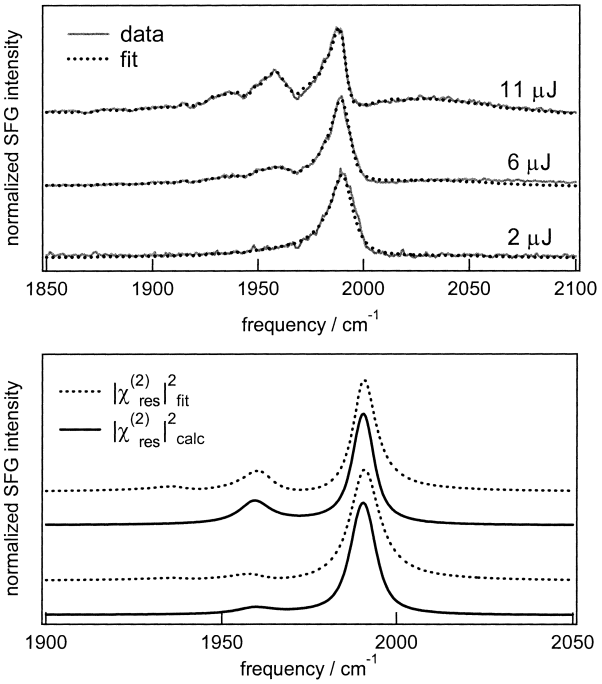

Fig. 1. Upper panel: Normalized SFG spectra of the CO-stretch of CO on Ru(001) as a function of IR energy at 95 K (solid grey lines) together with the least-squares fits to the data (dotted lines). Starting with an IR energy of 11 μJ at a coverage of about 0.007 ML a series of spectra was recorded as a function of decreasing IR energy while dosing CO via the background. At 11 μJ the fundamental and $v = 1 \rightarrow 2$ hot band transition are clearly visible. The third resonance is partly due to the $v = 2 \rightarrow 3$ hot band. Lower panel: Resonant part of the fit depicted in the upper panel for the 6 (lower trace) and 11 μJ (upper trace) experiments (dotted lines) and the results of the calculation (solid line) described in the text.

The resonant contributions to the transient spectra as well as the transient population in the excited states can be calculated with the density matrix formalism. In this formalism, a 3-level system is described by a (3×3)-matrix. The time-dependent polarizations associated with the ground ($v = 0 \rightarrow 1$) and excited state ($v = 1 \rightarrow 2$) transitions are related to the off-diagonal elements of the density matrix, as: $P(\omega) = e^{i\omega_{vis}t} \times Tr\,(\overline{\rho}\,\overline{\mu})$. The diagonal elements directly represent the relative population in the three levels (0, 1, 2). In the rotating frame, the equations of motion for the different matrix elements of $\overline{\rho}$ read:[23–25]

$$\dot{\tilde{\rho}}_{00} = -iV_{01}\tilde{\rho}_{10} + \text{c.c.} + \tilde{\rho}_{11}/T_1^{10} \quad (2)$$

$$\dot{\tilde{\rho}}_{01} = iV_{01}(\tilde{\rho}_{00} - \tilde{\rho}_{11}) + iV_{21}\tilde{\rho}_{02} - \tilde{\rho}_{01}\left[1/(2T_1^{10}) + 1/T_2^{01} + i\Omega_{01}\right] \quad (3)$$

$$\dot{\tilde{\rho}}_{11} = -iV_{12}\tilde{\rho}_{21} + \text{c.c.} + iV_{01}\tilde{\rho}_{10} + \text{c.c.} - \tilde{\rho}_{11}/T_1^{10} + \tilde{\rho}_{22}/T_1^{21} \quad (4)$$

$$\dot{\tilde{\rho}}_{12} = iV_{12}(\tilde{\rho}_{11} - \tilde{\rho}_{22}) - iV_{10}\tilde{\rho}_{02} - \tilde{\rho}_{12}\left[1/(2T_1^{10}) + 1/(2T_1^{21}) + 1/T_2^{12} + i\Omega_{12}\right] \quad (5)$$

$$\dot{\tilde{\rho}}_{02} = -i(V_{01}\tilde{\rho}_{12} - V_{12}\tilde{\rho}_{01}) - \tilde{\rho}_{02}\left[1/(2T_1^{21}) + 1/T_2^{02} + i\Omega_{20}\right] \quad (6)$$

The above equations are the independent equations for the density matrix elements. In addition we have:

$$\tilde{\rho}_{22} = 1 - \tilde{\rho}_{00} - \tilde{\rho}_{11} \quad (7)$$

$$\tilde{\rho}_{10} = \tilde{\rho}_{01}^{*};\ \tilde{\rho}_{21} = \tilde{\rho}_{12}^{*};\ \tilde{\rho}_{20} = \tilde{\rho}_{20}^{*} \quad (8)$$

In these equations, $\tilde{\rho}_{ij} = \rho_{ij}e^{i(\Omega_{ij})t}$ and the coupling matrix element $V_{ij} = -\mu_{ij}/(2\hbar)\varepsilon(t)$. T_1^{ab} and T_2^{ab} denote the population and pure dephasing lifetimes of transition $a \rightarrow b$, respectively. The detuning from the excitation resonance is given by $\Omega_{ij} = \omega_{ij} - \omega_{IR}$, μ_{ij} is the transition dipole moment of the transition from i to j and $\varepsilon(t)$ is the envelope of the incident IR field.

The set of Egs. 1–5 is solved using a fourth-order Runge–Kutta scheme, after decomposing Egs. 3–5 into their real and imaginary parts, resulting in 8 coupled differential equations. In these calculations, we set $T_1^{10} = T_1^{21}$, since the available phase-space for electron-hole pair creation in the relaxation processes are very similar, because almost the same amount of energy is involved in the two relaxation processes. We neglect population decay from the second excited state directly to the ground state, since the matrix element associated with this forbidden transition is expected to be very small. Furthermore, we set $\mu_{12} = 2\mu_{01}$, as for an harmonic oscillator,[26] with $\mu_{01} = 2.1 \times 10^{-30}$ Cm.[27] The T_2's are obtained from linewidth measurements of the fundamental transition (T_2^{01} corresponding to a linewidth of 3 cm^{-1},[13] hot band transitions (T_2^{12} corresponding to a linewidth of 15 cm^{-1},[21] and overtone transition (T_2^{02} corresponding to a linewidth of 6 cm^{-1},[28] as reported previously. Finally, the observed resonant part of the SFG spectrum can be calculated from $I_{res}(\omega) \propto |\chi_{res}^{(2)}|^2 \propto |P(\omega)|^2$, with the polarization $P(\omega) = e^{i\omega_{vis}t} \times Tr(\overline{\rho}\,\overline{\mu}) = e^{i\omega_{vis}t}\,[(\mu_{01}\rho_{10} - \mu_{10}\rho_{01}) + (\mu_{12}\rho_{21} - \mu_{21}\rho_{12})]$. The first two terms contain the signal at the fundamental transition ω_{01} and the second terms give rise to the signal at ω_{12}, the so-called hot-band transition ($v = 1 \rightarrow 2$). Here, we assume that the VIS-upconversion pulse is continuous wave. We account for the spectral width of the upconversion pulse and the instrumental resolution by convoluting the resultant spectra with a 5 cm^{-1} broad Gaussian. The vibrational lifetime T_1 of both excited states was set to be 2.0 ps in the calculations, as determined from previous time-resolved measurements for CO on other metal surfaces,[8,9] and from extrapolation of the linewidth to 0 K.[13]

The SFG light associated with the $v = 1 \rightarrow 2$ hot band transition is due to the interaction of the visible field with the infrared polarization ρ_{12}. The main pathway for generating ρ_{12} is: $\rho_{00} \rightarrow \rho_{01} \rightarrow \rho_{11} \rightarrow \rho_{12}$,[15] each arrow symbolizing one interaction with the incident IR field (note that in the equations (2)–(6) each of these terms has the preceding term multiplied by the infrared field (V_{ij}) as a source term). Hence, the polarization represented by ρ_{12} is of third order, and the additional interaction with the visible field makes it a fourth-order non-linear optical process.

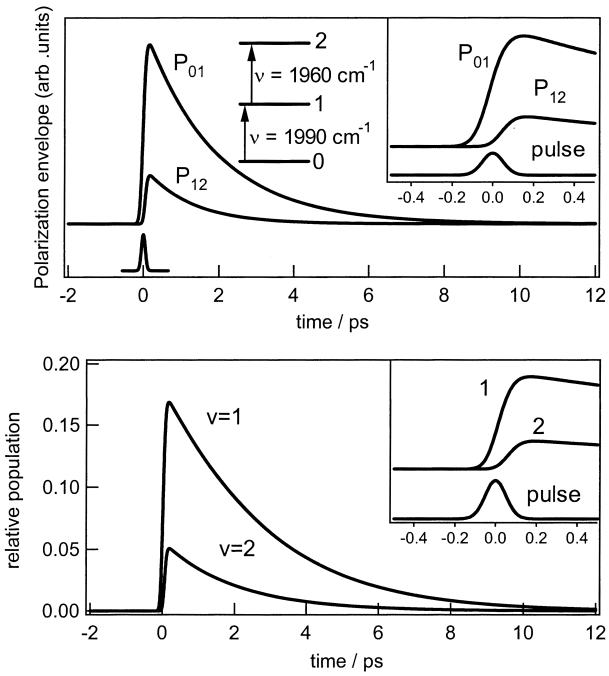

Fig. 2. Upper panel: Time-evolution of the polarization at the fundamental (P_{01}) and hot-band (P_{12}) transition. These calculations correspond to the 11 μJ data of Fig. 1. The insets depict the same data around time zero. Note the delayed rise of P_{12} compared to P_{01}. The pulse envelope is depicted around zero delay. Lower panel: Time-evolution of excited state population in the first and second excited state levels.

The calculated resonant contribution to the spectra in Fig. 1 are shown as solid lines in the lower panel, and the agreement with results from the fit to the resonant SFG (dotted lines) are excellent. The time-dependent envelopes of the polarization at the fundamental (P_{01}) and the hot-band (P_{12}) transition are depicted in the upper panel of Fig. 2 for the calculation that reproduces the 11μJ-experiment. The lower panel depicts the time evolution of the population in the first and second excited states. Note that, as expected, the rise of the polarization at the hot-band transition P_{12} is delayed with respect to that of the fundamental P_{01} (See inset in Fig. 2); This is due to the fact that the buildup of the polarization P_{12} arises from a sequence of interactions with the electromagnetic field: the initial interaction creates polarization P_{01}, and subsequently an additional interaction causes population to be transferred to $v = 1$. The third interaction with the IR field gives rise to P_{12}. The final, non-resonant interaction with the visible field creates the SFG from this vibrational polarization. For the same reason the population in $v = 2$ rises delayed when compared to the popu-

lation in the first excited state (lower panel of Fig. 2). Approximately 15% of the CO molecules is excited to the first vibrationally excited state, and about 5% to the second vibrationally excited state. The relatively large amount of population in $v = 2$ is due to the larger transition dipole moment associated with the $1 \rightarrow 2$ transition compared to the fundamental.

From the point of view of controlling the yield and pathway of reactions at surfaces by means of IR excitation, it is desirable to obtain maximal population in high-lying vibrational states. Provided these states are efficiently coupled to the relevant reaction coordinate, selective, vibrationally assisted chemistry may occur. Although the pulses used in this study are quite short (130 fs) and therefore quite intense, the spectral brightness of these pulses is relatively low because of the large bandwidth. To investigate the extent to which more population may be transferred using longer pulses, we calculated the pulse-duration dependence of the population and the SFG spectra, using the three-level Bloch equations.

In these calculations, the pulse energy was kept constant (at 200 μJ incident on a 1×10^{-5} m^2 surface area — reasonable experimental parameters, resulting in a fluence somewhat lower than in the experiments described above), and the pulse duration (full width at half maximum) was varied from 10 fs (ultrashort Ti:sapphire system) to 20 ps (actively and passively mode-locked Nd:YAG). The pulses are Gaussian and always bandwidth-limited. The system parameters (vibrational lifetimes, transition dipole moment) have been mentioned above. The anharmonicity was set at 30 cm^{-1}: the fundamental transition at 1990 cm^{-1} and the $1 \rightarrow 2$ hot-band transition at 1960 cm^{-1}, all in line with the experimental system described above. Unless otherwise mentioned, the central laser frequency was set at 1990 cm^{-1} — resonant with the fundamental transition.

Indeed, as can be observed in the upper panel of Fig. 3, a substantial gain in population transfer in both the first and second excited state can be achieved with longer excitation pulses due to the higher spectral brightness (depicted in the lower panel). In this figure, we have plotted the maximum value that is reached in time-traces such as those depicted in the lower panel of Fig. 2. For infinitely short pulses, the maximum population achieved is 0, since the laser spectrum is spread out too much to cause efficient excitation. The maximum population in the second excited state $v = 2$ is reached for a pulse duration of 400 fs, which is very close to the maximum in spectral brightness at the $1 \rightarrow 2$ hot-band transition located at 200 fs (see lower panel). A pulse duration of 400 fs corresponds to a bandwidth of 37 cm^{-1}. The $v = 1$ state population maximum is reached around 2 ps, which is determined by the finite lifetime of the excited state. This maximum is a consequence of the competition between increasing spectral brightness and vibrational relaxation that becomes more important for longer pulse durations. If the vibrational lifetime were longer, the maximum would be reached for longer pulses.

However, if one is interested in vibrationally mediated chemistry, the appropriate quantity to consider is the time-integrated population in the excited states, since one would monitor the time-integrated product yield, i.e. the integral of time-traces such as those depicted in the lower panel of Fig. 2. This is depicted in the upper panel of Fig. 4, which demonstrates two maxima in the $v = 2$ state as a function of pulse duration. This can be understood by noting that the pathway to the population in the second excited state ρ_{22} is: $\rho_{00} \rightarrow \rho_{01} \rightarrow \rho_{11} \rightarrow \rho_{12} \rightarrow \rho_{22}$. ρ_{22} can be maximized either by optimizing the first two steps (creating a large first excited state population ρ_{11}), or by optimizing the last two steps. The former requires high IR field intensities at the $0 \rightarrow 1$ transition frequency (optimized at a pulse duration of $\sim$ 2 ps), and the latter requires sufficient

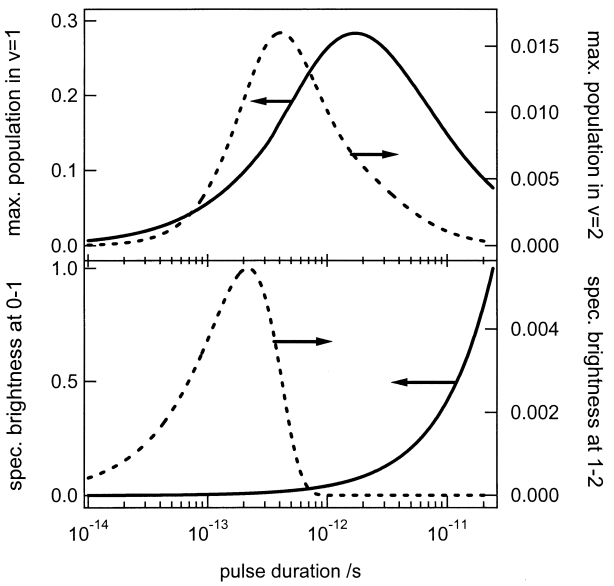

Fig. 3. Upper panel: Maximum population in the first and second excited state as a function of laser pulse duration. Lower panel: Spectral brightness at the fundamental (0–1) and hot band (1–2) transitions vs pulse duration.

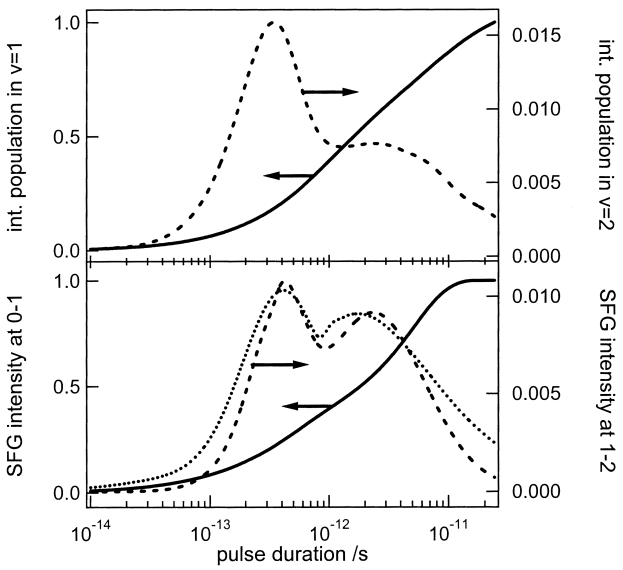

Fig. 4. Upper panel: Time-integrated population as a function of laser pulse duration. Lower panel: Integrated SFG intensity associated with a fundamental (0–1) and hot band (1–2) transitions vs. pulse duration. The dotted line in the lower panel depicts the larger of the (normalized) maximum population in $v = 1$ and $v = 2$; the envelope of the two curves in the upper panel of Fig. 3.

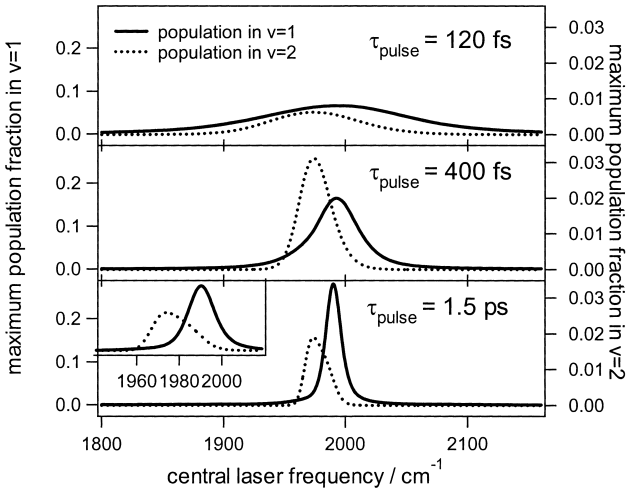

Fig. 5. Maximum population in the first and second excited state as a function of laser pulse central frequency, for three different pulse durations indicated in the graph. The associated spectral widths are 122, 37, and 9.8 cm^{-1}, respectively. The inset in the lower panel depicts a close-up of the 1.5 ps data, to illustrate the asymmetry of the $v = 2$ curve.

field strength at the $1 \rightarrow 2$ transition frequency (achieved for $t_p = 400$ fs).

A similar double-peaked behavior (with the same physical origin) is observed for the SFG intensity associated with the 1–2 transition (proportional to $|\rho_{12}|^2$), as shown in the lower panel of Fig. 4. Also shown is the SFG intensity of the fundamental transition (proportional to $|\rho_{01}|^2$). The dotted line in this graph illustrates the physical origin of the double-peaked behavior: it is the larger of the maximum population in $v = 1$ and $v = 2$, i.e. the larger of the two curves in the upper panel of Fig. 3. The similarity between the two curves demonstrates that efficiently exciting either one of the two transitions leads to a high overall excited state population.

These results indicate that even higher population transfer efficiency may be achieved using pulses with a central frequency in between the two transitions. Figure 5 demonstrates that this is indeed the case. Figure 5 depicts the maximum population in $v = 1$ and 2 as a function of the laser frequency for three different pulse duration: 120 fs, 400 fs, and 1.5 ps. The first observation is that, for all pulse durations, the maximum population in $v = 2$, the $v = 2$–peak, is located at 1974 cm^{-1}, i.e. within 1 cm^{-1} of the mean value of the the $v = 0 \rightarrow 1$ and the $v = 1 \rightarrow 2$ transitions. This demonstrates that in a two-step transition, optimal population transfer is achieved by setting the frequency in between the two individual transitions. The $v = 1$–peak is located at 1990 cm^{-1}, i.e. precisely at the frequency of the $v = 0 \rightarrow 1$ transition, as expected. The asymetry in the $v = 2$–data (present in all three curves, but most clearly for the 1.5 ps calculation, see inset) is again a consequence of the fact that large amounts of $v = 2$ population can be achieved either through excitation at the $v = 0 \rightarrow 1$ transition or in the neighborhood of $v = 1 \rightarrow 2$.

Conclusions

To summarize, femtosecond vibrational saturation spectroscopy of the CO-stretch vibration of CO/Ru(001) allows for the study of the dynamics of localized CO-stretch vibrations at CO coverages as low as 0.01 ML. The strong excitation (saturation) of the fundamental transition of the CO-stretch make the simultaneous observation of the fundamental and subsequent $v = 1 \rightarrow 2$ hot band transition possible. The considerable population transfer associated with these excited states spectra can be modeled with the density matrix formalism. The calculations demonstrate the competition between bandwidth (increasing with *decreasing* pulse duration) required to cover the anharmonicity of the vibration, and the spectral brightness (increasing with *increasing* pulse duration). We present some general guidelines for optimizing population transfer for vibrations. The presented analysis and general conclusions are not specifically for vibrations at surfaces, but should be relevant in condensed phase systems in general.

This work was supported in part by a fellowship for M. B. of the Royal Netherlands Academy of Arts and Sciences and by the Deutsche Forschungsgemeinschaft through SFB 450.

References

1 A. Sinha, M. C. Hsiao, and F. F. Crim, *J. Chem. Phys.*, **92**, 6333 (1990); *ibid.* **94**, 4928 (1991).

2 M. J. Bronikowski, W. R. Simpson, and R. N. Zare, *J. Chem. Phys.*, **97**, 2194 (1993); *ibid.* **97**, 2204 (1993).

3 R. B. Metz, J. D. Thoemke, J. M. Pfeiffer, and F. F. Crim, *J. Chem. Phys.*, **99**, 1744 (1993).

4 S. Chelkowski, A. D. Bandrauk, and P. B. Corkum, *Phys. Rev. Lett.*, **65**, 2355 (1990).

5 S. Chelkowski and A. D. Bandrauk, *Chem. Phys. Lett.*, **186**, 264 (1991).

6 D. J. Maas, D. I. Duncan, A. F. G. van der Meer, W. J. van der Zande, and L. D. Noordam, *Chem. Phys. Lett.*, **270**, 45 (1997).

7 S. M. Arrivo, T. P. Dougherty, W. T. Grubbs, and E. J. Heilweil, *Chem. Phys. Lett.*, **235**, 247 (1995).

8 J. D. Beckerle, R. R. Cavanagh, M. P. Casassa, E. J. Heilweil, and J. C. Stephenson, *J. Chem. Phys.*, **95**, 5403 (1991).

9 M. Morin, N. J. Levinos, and A. L. Harris, *J. Chem. Phys.*, **96**, 3950 (1992).

10 Y. R. Shen, *Nature*, **337**, 519 (1989), and references therein.

11 D. J. Maas, D. I. Duncan, R. B. Vrijen, W. J. van der Zande, and L. D. Noordam, *Chem. Phys. Lett.*, **290**, 75 (1998).

12 V. D. Kleiman, S. M. Arrivo, J. S. Melinger, and E. J. Heilweil, *Chem. Phys.*, **233**, 207 (1998).

13 P. Jakob and B. N. J. Persson, *Phys. Rev.*, **B 56**, 10644 (1997).

14 Ch. Hess, M. Wolf, and M. Bonn, *Phys. Rev. Lett.*, **85**, 4341 (2000).

15 M. Bonn, Ch. Hess, and M. Wolf, *J. Chem. Phys.*, **115**, 7725 (2001).

16 E. W. M. van der Ham, Q. H. F. Vrehen, and E. R. Eliel, *Opt. Lett.*, **21**, 1448 (1996).

17 L. J. Richter, T. P. Petralli-Mallow, and J. C. Stephenson, *Opt. Lett.*, **23**, 1594 (1998).

18 M. Bonn, Ch. Hess, S. Funk, J. H. Miners, B. N. J. Persson, M. Wolf, and G. Ertl, *Phys. Rev. Lett.*, **84**, 4653 (2000).

19 S. Funk, M. Bonn, D. N. Denzler, Ch. Hess, M. Wolf, and G. Ertl, *J. Chem. Phys.*, **112**, 9888 (2000).

20 H. Pfnür, P. Feulner, and D. Menzel, *J. Chem. Phys.*, **79**, 4613 (1983).
21 Ch. Hess, M. Bonn, S. Funk, and M. Wolf, *Chem. Phys. Lett.*, **325**, 139 (2000).
22 J. H. Hunt, P. Guyot-Sionnest, and Y. R. Shen, *Chem. Phys. Lett.*, **133**, 189 (1987).
23 A. L. Harris and L. Rothberg, *J. Chem. Phys.*, **94**, 2449 (1991).
24 E. Knoesel, A. Hotzel, and M. Wolf, *J. Electron. Spectrosc. Relat. Phenom.*, **88-91**, 577 (1998).
25 R. W. Boyd, "Non-linear Optics," Academic Press, San Diego (1992), p. 191.
26 P. W. Atkins, "Physical Chemistry," 4th ed., Oxford University Press, Oxford (1990).
27 P. Jakob, private communication.
28 P. Jakob and B. N. J. Persson, *J. Chem. Phys.*, **109**, 8641 (1998).